Increase in venous thromboembolism in SARS-CoV-2 infected lung tissue: proteome analysis of lung parenchyma, isolated endothelium, and thrombi

Boaz V Lopuhaä,[1] Coşkun Guzel,[2] Anabel van der Lee,[3] Thierry P P van den Bosch,[1] Folkert J van Kemenade,[1] Menno V Huisman,[4] Marieke J H A Kruip,[5] Theo M Luider[2] & Jan H von der Thüsen[1]

[1]Department of Pathology, [2]Laboratory of Neuro-Oncology, Clinical and Cancer Proteomics, Department of Neurology, Erasmus University Medical Centre, Rotterdam, [3]Vrije Universiteit, Amsterdam, [4]Department of Thrombosis and Hemostasis, Leiden University Medical Center, Leiden and [5]Department of Haematology, Erasmus University Medical Centre, Rotterdam, the Netherlands

Lopuhaä B V, Guzel C, van der Lee A, van den Bosch T P P, van Kemenade F J, Huisman M V, Kruip M J H A, Luider T M & von der Thüsen J H

(2024) Histopathology. https://doi.org/10.1111/his.15143

Increase in venous thromboembolism in SARS-CoV-2 infected lung tissue: proteome analysis of lung parenchyma, isolated endothelium, and thrombi

Aims: COVID-19 pneumonia is characterized by an increased rate of deep venous thrombosis and pulmonary embolism. To better understand the pathophysiology behind thrombosis in COVID-19, we performed proteomics analysis on SARS-CoV-2 infected lung tissue.

Methods: Liquid chromatography mass spectrometry was performed on SARS-CoV-2 infected postmortem lung tissue samples. Five protein profiling analyses were performed: whole slide lung parenchyma analysis, followed by analysis of isolated thrombi and endothelium, both stratified by disease (COVID-19 versus influenza) and thrombus morphology (embolism versus in situ). Influenza autopsy cases with pulmonary thrombi were used as controls.

Results: Compared to influenza controls, both analyses of COVID-19 whole-tissue and isolated endothelium showed upregulation of proteins and pathways related to liver metabolism including urea cycle activation, with arginase being among the top upregulated proteins in COVID-19 lung tissue. Analysis of isolated COVID-19 thrombi showed significant downregulation of pathways related to platelet activation compared to influenza thrombi. Analysis of isolated thrombi based on histomorphology shows that *in situ* thrombi have significant upregulation of coronavirus pathogenesis proteins.

Conclusions: The decrease in platelet activation pathways in severe COVID-19 thrombi suggests a relative increase in venous thromboembolism, as thrombi from venous origin tend to contain fewer platelets than arterial thrombi. Based on histomorphology, *in situ* thrombi show upregulation of various proteins related to SARS-CoV-2 pathogenesis compared to thromboemboli, which may indicate increased *in situ* pulmonary thrombosis in COVID-19. Therefore, this study supports the increase of venous thromboembolism without undercutting the involvement of *in situ* thrombosis in severe COVID-19.

Keywords: COVID-19, *in situ* thrombosis, proteomics, thromboembolism, thrombosis

Address for correspondence: B V Lopuhaä, Department of Pathology, Erasmus MC, Doctor Molewaterplein 40, Rotterdam 3015GD, the Netherlands. e-mail: b.lopuhaa@erasmusmc.nl

Introduction

The pandemic of COVID-19 was characterized by an excessive mortality rate. In 2020, the World Health Organization reported approximately 1.8 million confirmed deaths attributable to the COVID-19 pandemic, but estimated this number to be at least 3 million due to underreporting.[1] Influenza, a viral disease with similar transmission and pulmonary complaints, has lower annual deaths, presumed to be between 0.2 and 0.5 million.[2] In fact, mortality of hospitalized patients was 10 times higher for COVID-19 compared to influenza.[3] The high frequency of thrombotic complications seen in COVID-19 contributes significantly to the high mortality, especially when compared with influenza.[4,5] *In situ* pulmonary arterial thrombosis as well as classic pulmonary thromboemboli—mostly originating in the leg veins—have been associated with SARS-CoV-2.[5,6] An increase in complement activation, cytokine storms, and vascular permeability play a vital role in COVID-19 thrombosis,[7] although activation of these pathways is also present in influenza.[8,9] The reason why this increase of the abovementioned pathways in thrombosis seems more activated in COVID-19 than in influenza is unclear. We studied protein composition through use of liquid chromatography–mass spectrometry (LC-MS) in thrombosis of COVID-19 postmortem SARS-CoV-2 infected lung tissue. We compared profiles with postmortem lung tissue samples from influenza cases. Sequentially, LC-MS was performed on isolated thrombi and endothelium of the same groups to improve the identification of proteins related to thrombosis. Lastly, analyses were performed on isolated thrombi and surrounding endothelium based on thrombus histomorphology (*in situ* thrombus or thromboembolus) independent of underlying disease to gain insight into –mechanisms behind both phenotypes of thrombosis.

Materials and Methods

TISSUE ACQUISITION AND HISTOLOGICAL EXAMINATION

Postmortem lung tissue from 19 autopsies in the Erasmus University Medical Center was selected for LC-MS. These included eight COVID-19 autopsies and 11 consecutive influenza pneumonia autopsies (Table 1). The COVID-19 cases had been tested positive for SARS-CoV-2 by polymerase chain reaction (PCR), both by nasal swab up to 1 month before death as well as postmortem swabs of both main bronchi. Influenza cases were included if the autopsy report mentioned influenza as (contributory) cause of death. All influenza cases were tested positive for influenza type A or B through partial sequencing of reverse-transcriptase-PCR of lung tissue or nasopharyngeal swab; one influenza case had an increased titre of influenza antibodies. COVID-19 autopsies were from 2020, during the first wave of the alpha variant in the Netherlands. Influenza autopsies were carried out between 1993 and 2019. All autopsies were carried out in the Erasmus University Medical Center in Rotterdam. Consent was by the next of kin to utilize postmortem organ tissue from autopsies for research purposes. Permission for utilization of COVID-19 tissue samples was granted by the Medical Ethics Review Committee (MEC-2020-0322).

WHOLE-TISSUE ANALYSIS

For whole-tissue analysis, formalin-fixed and paraffin-embedded (FFPE) samples of lung tissue were selected from five available COVID-19 cases and all 11 influenza cases. FFPE sample selection was performed on corresponding haematoxylin and eosin (HE)-stained slides, of which one slide with the most extensive diffuse alveolar damage was selected for proteomics analysis. Each slide was then scored for the presence of histomorphological features indicative for diffuse alveolar damage (DAD) in a semiquantitative 3-point scoring system indicating absence (0), low,[1] medium,[2] or high[3] presence (Table 2). These features include hyalin membranes, haemorrhage, alveolar histiocytes, fibrosis, acute fibrinous, and organizing pneumonia (AFOP) and pneumocyte hyperplasia (Figure 1). Slides available per case for this selection varied between 2 to 20 slides. Then, for each selected FFPE lung tissue sample a consecutive slide following the HE-stained slide was cut and processed for LC-MS (see: Processing, below). Cases for whole-tissue analysis were grouped based on disease as either COVID-19 or influenza.

LASER CAPTURE MICRODISSECTION

For the laser capture microdissection (LCM) analyses, all lung tissue slides from all cases were examined for the presence of thrombi. Samples from four COVID-19 cases and five influenza cases used for whole-tissue analysis had (micro)thrombi and were eligible for LCM analysis. Samples from three other COVID-19 cases with (micro)thrombi were added for LCM analyses to increase the group size. Each case was labelled for disease and thrombus type. Protein

Table 1. Patient characteristics

Study ID	Analysis	Disease	Sex	Age	Medical history	Summary of clinical course	BMI	IS	AC	AV	DI	LOS H	LOS ICU	VE	Thrombus type
1	WT	COVID-19	M	65	Blank	Progressive respiratory decline with intubation, tracheotomy 13 days before death after unsuccessful extubation, multiple pulmonary embolisms 5 days before death, cardiac arrest	26.0	–	Heparin	–	28	28	24	21	–
2	WT	Influenza (variant unknown[a])	M	44	Cardiomyopathy with VVI-pacemaker, decompensatio cordis, diabetes mellitus, obesity	Fever, diabetic coma with severe dehydration, liver failure, anaemia, pneumonia, hyperthyroidism, sudden loss of tension	30.4	n.a.[a]	n.a.[a]	n.a.[a]		14	n.a.[a]	n.a.[a]	–
3	WT	Influenza (IAV)	M	3	Transposition of the great vessels, atrial septal defect, ventricular septal defect	Fever, rhinitis, found lifeless in bed	n.a.[a]	n.a.[a]	n.a.[a]	n.a.[a]	7	5	0	0	–
4	WT	Influenza (IAV)	F	22	B- and T-cell acute lymphoblastic leukaemia, graft versus host disease of skin and liver, HSV and RSV superinfection, bronchitis obliterans organizing pneumonia	Dyspnea before admission. Influenza H1N1 infection, progressive respiratory deterioration, pneumothorax	n.a.[a]	Prednisolon: unspecified dose[a]	n.a.[a]	n.a.[a]	9	9	9	7	In situ
5	WT	Influenza (IAV)	F	15	Blank	Progressive respiratory decline, influenza, s. aureus and pseudomonas infection, aspiration pneumonia	20.4	–	Heparin	–	42	38	37	37	–
6	WT	Influenza (IAV)	M	17	Blank	Respiratory insufficiency, septic shock, intubation, kidney- and liver failure, encephalopathy	15.4	–	–	–	44	39	34	34	–
7	WT	Influenza (IAV)	M	2	Blank	Vomiting, diarrhoea, loss of consciousness, failed resuscitation	n.a.[a]	–	–	–	6	0	0	0	–
8	LCM	COVID-19	M	70	Hypothermia, autonomic dysregulation	Progressive respiratory decline, renal failure, pulmonary hypertension, anaemia	20.0	–	–	–	3	3	0	0	Embolism
9	LCM	COVID-19	F	70	Kidney infarct, sicklecelltrait, cholecystectomy, CVA, hypertension, Diabetes mellitus	Found lifeless at home, persistent abdominal pain after cholecystectomy 2 weeks before death	27.1	–	–	–	4	0	0	0	Embolism
10	LCM	COVID-19	M	54	Chronic renal insufficiency, arteriovenous shunt left arm, anaemia, secondary hypoparathyroidism, hypertension, obesity, gout	Progressive respiratory deterioration, hypokalemia	27.3	–	Heparin	–	17	10	10	7	Embolism

Table 1. (*Continued*)

Study ID	Analysis	Disease	Sex	Age	Medical history	Summary of clinical course	BMI	IS	AC	AV	DI	LOS H	LOS ICU	VE	Thrombus type
11	WT & LCM	COVID-19	M	66	Chronic limb ischemia, hypertension, obesity	Dyspnea and fever before admission. Progressive respiratory deterioration, acute renal failure, liver failure	35.9	–	Dalteparin	Lopinavir, ritonavir	12	11	9	8	In situ
12	WT & LCM	COVID-19	M	52	Myocardial infarction, hypertension, diabetes mellitus type 2, obesity	Dyspnea before admission. Progressive respiratory deterioration, pulmonary embolisms	37.6	–	Heparin	–	12	10	6	6	Embolism
13	WT & LCM	COVID-19	M	67	Angina pectoris, obesity	Dyspnea before admission. Progressive respiratory deterioration, pulmonary embolisms, pneumomediastinum, HSV and aspergillus abscesses	30.3	–	Heparin	Acyclovir	30	27	23	19	Embolism
14	WT & LCM	COVID-19	M	72	Diabetes mellitus type 2	Dyspnea and fever before admission. Progressive respiratory deterioration, pulmonary embolisms, mucus stasis, acute renal failure	24.8	–	Heparin	–	36	22	21	21	In situ
15	WT & LCM	Influenza (IBV)	F	1	Acute myeloblastic leukaemia, Down syndrome	Progressive respiratory deterioration, cholestasis, diffuse intravascular coagulation	n.a.[a]	n.a.[a]	n.a.[a]	n.a.[a]	34	22	22	18	Embolism
16	WT & LCM	Influenza (IBV)	M	3	Ménétrier's disease	Clostridium infection, sepsis, progressive respiratory deterioration	n.a.[a]	n.a.[a]	n.a.[a]	n.a.[a]	n.a.[a]	n.a.[a]	n.a.[a]	n.a.[a]	In situ
17	WT & LCM	Influenza (IAV)	F	64	Blank	Fever, dyspnea, intubation pneumosepsis, influenza and candida albicans infection, bradycardia, renal insufficiency, asystole	28.7	–	Heparin	–	33	26	26	23	Embolism
18	WT & LCM	Influenza (IAV)	M	43	Tuberculosis, rheumatoid arthritis, chronic lymphoid leukaemia	Coughing, fever, progressive respiratory insufficiency	24.5	Prednisolon: 80 mg	–	Oseltamivir	24	21	17	17	Embolism
19	WT & LCM	Influenza (IAV)	F	48	ANCA+ vasculitis	Months of coughing and since 1 day before admission fever. Progressive respiratory deterioration, pneumothorax	20.4	Prednisolon: 60 mg for 26 days; 30 mg for 11 days; Patient died during treatment	–	–	21	20	20	13	In situ

AC, Anticoagulants; AV, Antivirals; DI, Days of illness before death; IAB, Influenza B virus; IAV, Influenza A virus; IS, Immunosuppressants; LCM, Laser microdissection analysis; LOS H, Length of stay in hospital; LOS ICU, Length of stay on the intensive care unit; VE, Days on ventilation; WT, Whole tissue analysis.

[a]Medical reports did not disclose information regarding this variable.

Table 2. Diffuse alveolar damage grading. Each case was graded in a semiquantitative 3-point scoring system indicating absence (0), low (1), medium (2), or high (3) presence of features indicative for DAD

| Study ID	Disease	Hyalin membranes	Haemorrhage	Alveolar histiocytes	Fibrosis	AFOP	Pneumocyte hyperplasia	DAD phase
1	COVID-19	0	0	3	2	0	3	Chronic
2	Influenza	1	1	1	0	0	0	Acute
3	Influenza	0	1	2	0	0	2	Acute
4	Influenza	3	3	1	1	1	0	Acute
5	Influenza	0	3	1	2	2	2	Acute
6	Influenza	0	3	3	0	0	3	Acute
7	Influenza	0	0	0	0	0	3	Acute
8	COVID-19	2	1	2	1	0	2	Acute
9	COVID-19	2	1	1	0	0	2	Acute
10	COVID-19	1	0	1	0	0	2	Acute
11	COVID-19	2	3	2	1	3	1	Acute
12	COVID-19	1	1	3	1	3	1	Acute
13	COVID-19	1	1	1	3	0	0	Chronic
14	COVID-19	3	1	2	3	2	0	Chronic
15	Influenza	1	1	3	2	0	1	Chronic
16	Influenza	0	3	1	3	0	0	Chronic
17	Influenza	3	2	2	0	2	0	Acute
18	Influenza	1	2	2	2	0	1	Chronic
19	Influenza	1	2	3	1	0	1	Acute

profiling analyses performed on isolated thrombi and endothelium were then stratified by disease (either "COVID-19" or "influenza") and thrombus type (either "*in situ* thrombus" or "thromboembolus"). The distinction between *in situ* thrombi and thromboemboli was based on histomorphological appearance independent of underlying disease. Thrombi were considered to be *in situ* if the thrombus showed eccentric inward growth from the vessel wall towards the lumen. If the majority of the thrombus surface was not connected to the vessel wall, but consisted of a considerable amount of erythrocytes and/or showed layered formation of fibrin and erythrocytes (layers of Zahn), the thrombus was categorized as a thromboembolus (Figure 2).

To meet the minimum requirement of material for LCM analysis, a minimum surface of 800,000 μm^2 of material was dissected from 10-μm-thick slides from both thrombi and endothelium, prepared on polyethylene naphthalate (PEN) membrane-covered microscopic slides (Carl Zeiss, Zwijndrecht, the Netherlands). For LCM analysis of endothelium, strips of vessel wall containing endothelium were dissected, extending up to 50 μm into the intima and media, as single endothelial cells could not be dissected because of the thickness of the laser cut. Thrombi and surrounding endothelium were captured from the same slide. For both thrombus and endothelium isolation, additional consecutive slides were cut for LCM if the material from one slide was deemed to be insufficient.

PROCESSING

Material from both whole-tissue and LCM analyses were analysed with LC-MS after deparaffinization, xylene removal, de-crosslinking, solubilizing, and
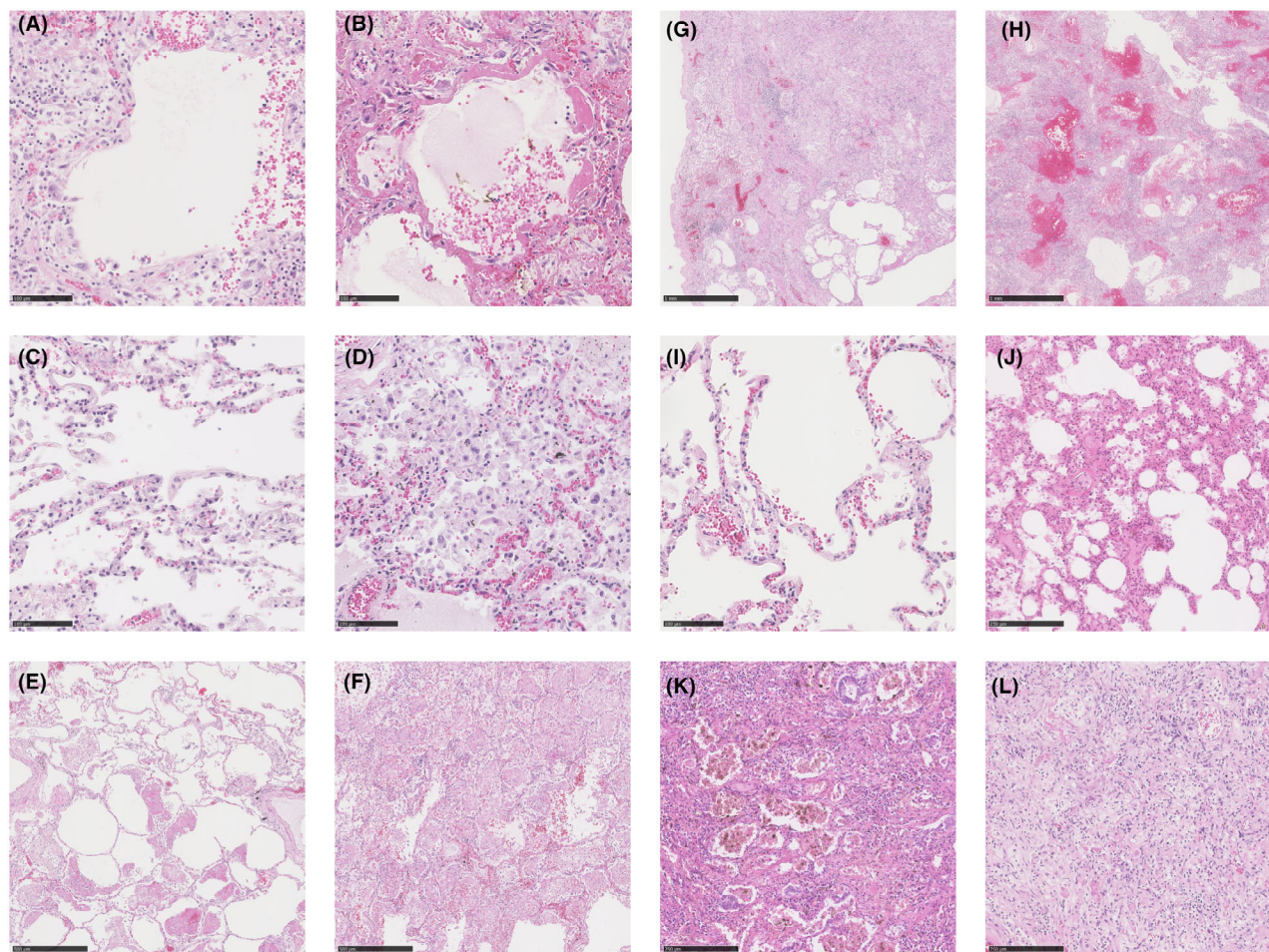
Figure 1. Examples of mild to severe histopathological characteristics of diffuse alveolar damage. These include hyaline membranes (A,B), alveolar histiocytes (C,D), acute fibrinous, and organizing pneumonia (AFOP) (E,F), haemorrhage (G,H), pneumocyte hyperplasia (I,J), and fibrosis (K,L). For each displayed feature, left examples portray the mild presence of said feature (score 1) and right examples portray the severe presence (score 3). The severity of each feature varied between COVID-19 and influenza cases; the displayed examples originated from both COVID-19 (A,B,C,E,F,I,L) and influenza cases (D,G,H,J,K).

digestion. Samples were loaded onto a trap column (PepMap C18, 300 μm ID, 5 mm length, 5 μm particle size, 100 Å pore size; ThermoFisher Scientific, Waltham, MA, USA), washed, and desalted for 8 min using 0.1% trifluoroacetic acid as the loading solvent at a flow rate of 20 μl/min. The trap column was switched in-line with the analytical column (PepMap C18, 75 μm ID × 500 mm, 2 μm particle size, and 100 Å pore size, ThermoFisher Scientific) and peptides were eluted with a 90-min acetonitrile gradient ranging from 3% to 30% (and formic acid concentration from 0.1% to 0.08%, respectively). All LC solvents were purchased from Biosolve (Valkenswaard, the Netherlands). The column flow rate was set to 250 nl/min, and eluting peptides were measured at 214 nm in a 3 nl nano flow cell (ThermoFisher

Scientific), coupled online to the mass spectrometer. For electrospray ionization nano ESI emitters (New Objective, Woburn, MA, USA) were used and a spray voltage of 1.7 kV was applied. For MS detection, a data-dependent acquisition method was used with a survey scan from 350 to 1650 Th at 120,000 resolution (AGC target 400,000) and consecutively isolated and fragmented by collisional induced dissociation (CID) at 35% normalized collision energy (AGC target 10,000) of the most abundant precursors in the linear ion trap until a duty cycle time of 3 s was reached ('Top Speed' method). Precursor masses that were selected once for MS/MS were excluded from further fragmentation for the next 60 s.

Proteins from the LCM-derived samples were assigned by exporting features, for which MS/MS
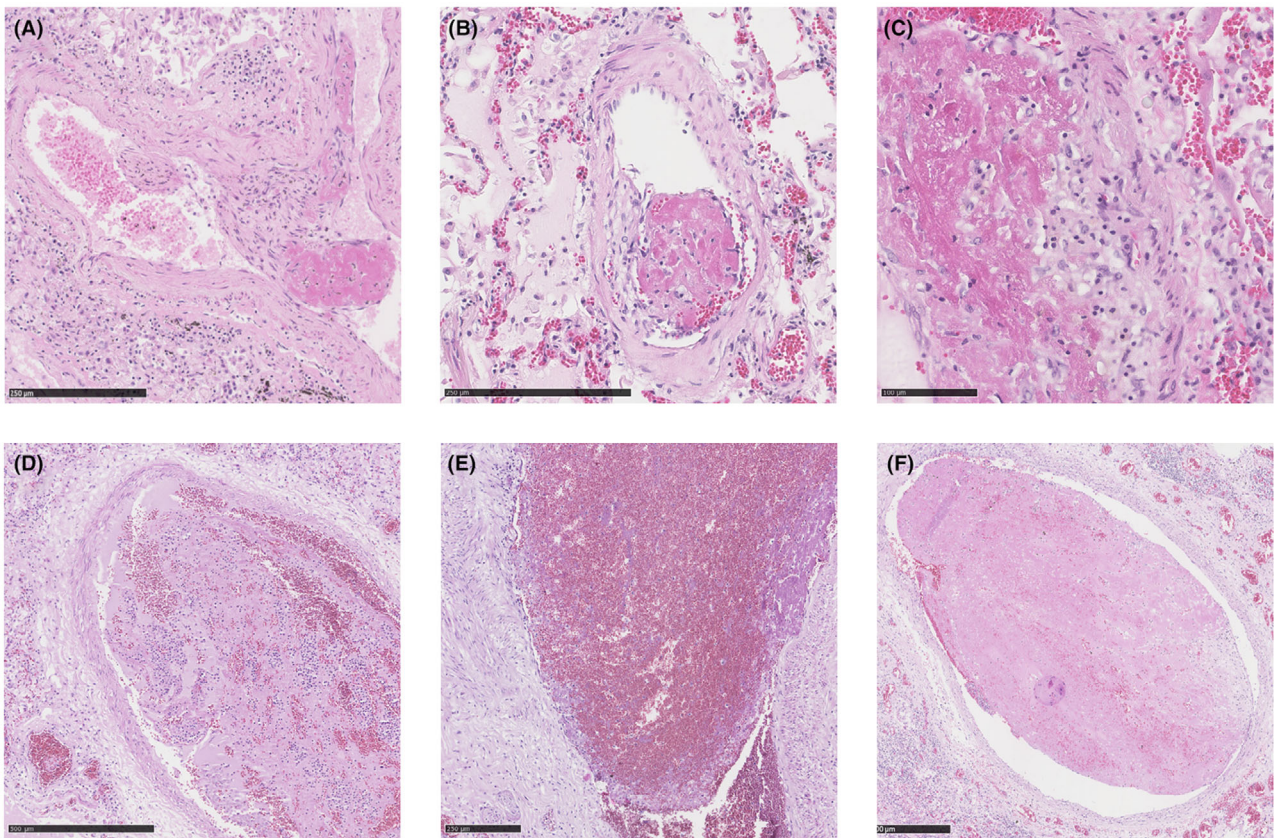
Figure 2. Examples of pulmonary thrombi. *In situ* thrombi (A–C) show inward growth of thrombus from the vascular wall towards the lumen. Proliferation of fibroblasts (A,B) and vascular infiltration of lymphocytes (C) were seen in *in situ* thrombi. Thromboemboli (D–F) are virtually unconnected to the vascular wall. Thromboemboli consisted of a considerable amount of erythrocytes, occasionally forming layers of fibrin and erythrocytes; lines of Zahn (F).

spectra were recorded, using the ProteoWizard software (v. 3.0.9248; http://proteowizard.sourceforge.net). The resulting .mgf files were submitted to Mascot (v. 2.3.01, Matrix Science, London, UK) and applied to the human database (UniProtKB/Swiss-Prot, v. 2013_07, human taxonomy, 20,265 entries) for protein identifications assuming trypsin digestion and applying the following parameters: fragment ion mass tolerance of 0.50 Da, parent ion mass tolerance of 10 ppm, and the maximum number of missed cleavages was set to two. Oxidation of methionine was specified in Mascot as a variable modification, while carbamidomethylation of cysteine was set as a fixed modification.

DATA ANALYSIS

Scaffold (v. 5.1.2, Proteome Software, Portland, OR, USA) was used to summarize and filter the MS/MS-based peptide data from all Mascot searches. The number of proteins was derived from the peptide data according to the following criteria. Peptide identifications needed to have more than 95% probability, as specified by the Peptide Prophet algorithm. Protein identifications had to have more than 99% probability and contain at least one peptide identified. Proteins with zero counts after normalization were removed. For each individual protein, an analysis of variance (ANOVA) test was used to determine statistical significance in difference. Fold change was determined by calculating the ratio between means of normalized values per unique identified protein. Ingenuity Pathway Analysis (IPA) (Qiagen, Hilden, Germany) was used to interpret data by connecting proteins to signalling pathways. Activation or inhibition of pathways was indicated with z-scores; z-scores <-2 or >2 were respectively considered as an inhibition or activation. Pathways were eligible for z-score calculation if a minimum of four proteins and/or peptides related to said pathway were identified with a $P < 0.05$.

Results

WHOLE-TISSUE ANALYSIS

Whole-tissue analysis identified a total of 4452 different proteins among all samples after removal of proteins or peptides with zero counts after normalization. On average, 2231 different proteins and peptides were identified per sample, ranging between 1794 and 2451 without statistical difference between COVID-19 and influenza cases. In total, 356 proteins were differentially expressed between COVID-19 and influenza samples ($P < 0.050$), of which 27 were upregulated in COVID-19 (Table 3).

A full list of identified proteins per analysis is displayed in Table S1.

Whole-tissue analysis shows significant upregulation of 37 identified pathways in COVID-19 compared to influenza, including upregulation of ephrin receptor signalling and histamine degradation. A significant portion of these pathways were related to metabolic processes taking place in the liver, among which the urea cycle pathway (Figures 3A and 4). Nearly half of the identified upregulated pathways (14/37) had involvement of aldehyde dehydrogenases. A full list of up- and downregulated pathways per analysis is displayed in Table S2. No significant

Table 3. Identified proteins and pathways in performed analyses

	Whole tissue analysis: INF versus COV	LCM–thrombi: INF versus COV	LCM–endothelium: INF versus COV	LCM–thrombi: EMB versus INS	LCM–endothelium: EMB versus INS
Total identified proteins	4452	2463	2366	2463	2366
Differentially expressed proteins[a]	296 (26/270)	127 (31/96)	149 (53/98)	54 (12/42)	38 (14/24)
Total identified pathways	478	388	306	150	42
Differentially expressed pathways[a]	37 (0/37)	92 (87/5)	2 (1/1)	2 (1/1)	0
Top 5 upregulated pathways in INF	No upregulated pathways	Integrin signalling IL-8 signalling Actin nucleation by ARP-WASP Complex RAC signalling FAK signalling	CSDE1 signalling	–	–
Top 5 upregulated pathways in COV	Xenobiotic metabolism PXR Signalling pathway Serotonin degradation Noradrenaline and Adrenaline degradation Ethanol degradation II Neutrophil extracellular trap signalling	PPARα/RXRα activation PTEN signalling Serotonin degradation CLEAR signalling Ethanol degradation II PPAR signalling	DHCR24 signalling	–	–
Top 5 upregulated pathways in EMB	–	–	–	EIF2 signalling	No upregulated pathways
Top 5 upregulated pathways in INS	–	–	–	Coronavirus pathogenesis pathway	No upregulated pathways

Proteins were considered differentially expressed if $P < 0.050$. Top five upregulated pathways were based on highest and lowest Z-scores per analysis. Pathways were considered differentially expressed if Z-scores were >2 or <−2. INF: influenza cases. COV, COVID-19 cases; EMB, thromboembolism cases; INS, *in situ* thrombi cases.
[a]Down- and upregulated proteins or pathways per analysis are displayed in parentheses.
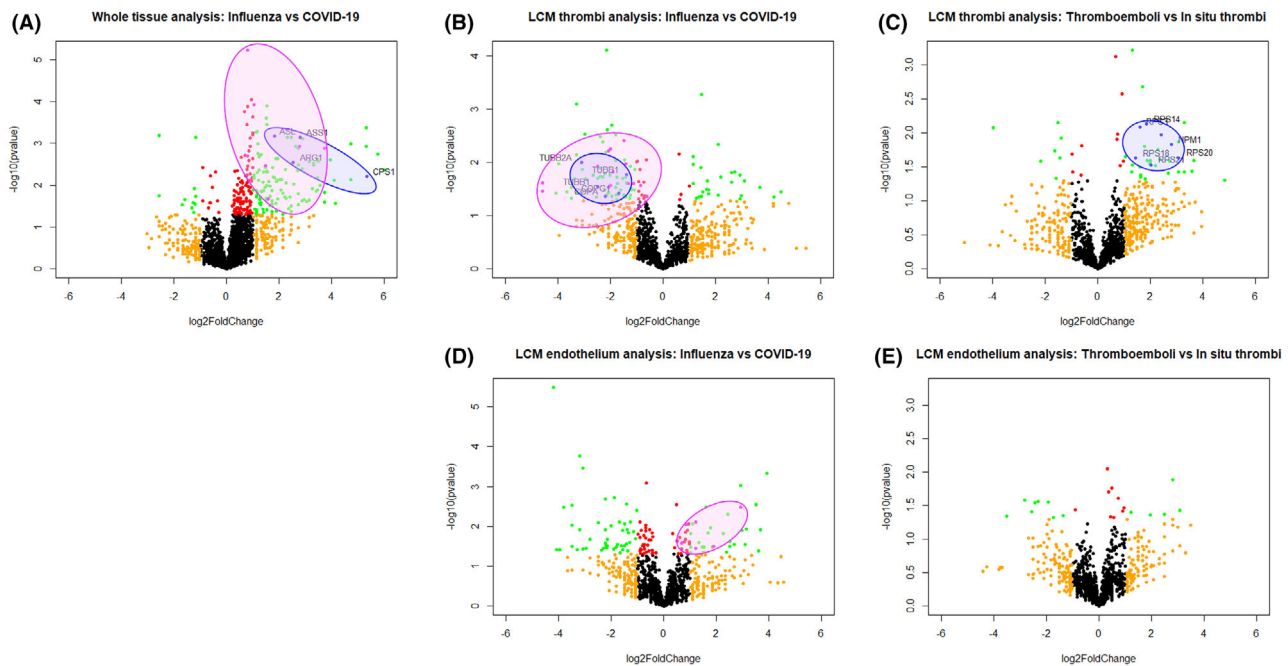
Figure 3. Volcano plots showing differentially expressed proteins in whole-tissue analysis and LCM analysis. Each dot represents a unique protein or peptide. Green dots represent proteins and peptides with a *P*-value <0.05 and a fold change <−1 or >1 and were considered differentially expressed. Highlighted proteins are displayed with corresponding gene name. (A) Whole-tissue analysis of influenza versus COVID-19. Blue dots represent upregulated proteins participating in the urea cycle, magenta represents proteins involved with histamine degradation. (B) LCM analysis of influenza and COVID-19 thrombi. Blue dots represent proteins related to COVID-19 replication. Magenta dots represent proteins related to integrin signalling. The majority of these proteins were also related to thrombin, CXCR4, PAK, paxilin, and ephrin signalling pathways. (C) LCM analysis of thromboemboli and *in situ* thrombi. Blue dots represent proteins related to the coronavirus pathogenesis pathway, upregulated in *in situ* thrombi. (D) LCM analysis of endothelium between influenza versus COVID-19. Magenta dots represent upregulated proteins in COVID-19 involved with DHCR24 signalling; a key pathway of cholesterol synthesis. (E) LCM analysis of endothelium from cases with thromboemboli and *in situ* thrombi. No differentially expressed pathways were identified.

upregulated pathways were identified in influenza compared to COVID-19.

LASER CAPTURE MICRODISSECTION ANALYSIS: THROMBI

Protein profiling of isolated thrombi identified 2463 different proteins and peptides with on average 1026 per sample, ranging between 356 and 1421 different proteins and peptides. LCM analysis of thrombi based on underlying disease showed 127 differentially expressed proteins between COVID-19 and influenza thrombi. LCM analysis of thrombi based on histomorphology showed 54 differentially expressed proteins between *in situ* thrombi and thromboemboli (Table 3).

Pathway analysis showed five upregulated pathways and 87 downregulated pathways in COVID-19 thrombi compared to influenza thrombi. Integrin- and interleukin-8 signalling were among the most downregulated pathways, with respective z-scores of

−3.05 and −3.00 (Figures 3B and 5). Other pathways related to inflammatory response (signalling pathways of: interleukin 3/8/17, Fc Epsilin RI. HMGB1, phospholipase C, STAT3, NF-kB) and platelet activity (signalling pathways of: TGF-beta, thrombin, paxilin, ephrin, PAK, and CXCR4) were also downregulated in COVID-19 thrombi. Lastly, five proteins related to the coronavirus replication pathway were downregulated in COVID-19 thrombi. These were: COPI coat complex subunits alpha and gamma 1 (*COPA* and *COPG1*) and tubulin proteins beta 1 class VI, beta 6 class V, and beta 2a class IIa (*TUBB1, TUBB6* and *TUBB2A*) (Figures 3B and 6A). Analysis of proteins related to specific diseases and functions revealed a significant increase in functions associated with thrombocytopenia, bleeding time, and lung inflammation. A decrease in proteins associated with viral infection was found in COVID-19 thrombi.

Between *in situ* thrombi and thromboemboli, two pathways showed significant differential expression,
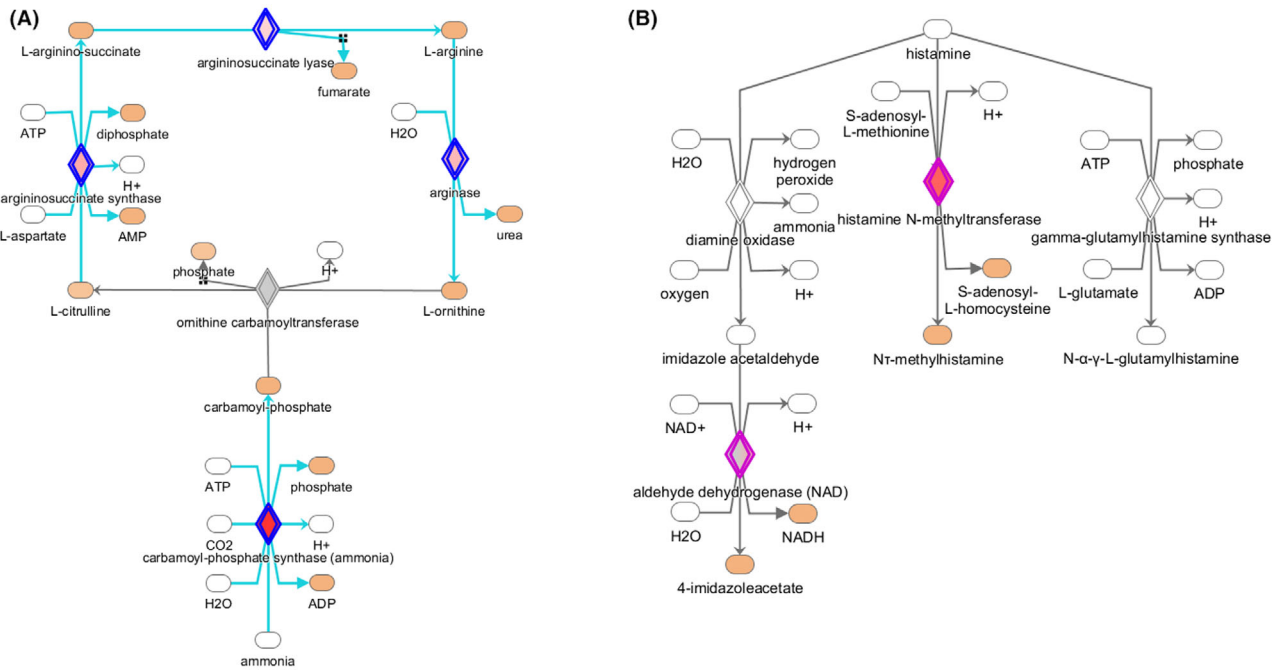
Figure 4. Whole-tissue analysis pathway examples. (A) Urea cycle pathway. Four proteins were found to be upregulated in COVID-19 lung tissue, represented by blue framed diamonds. Intensity of the orange colour represents predicted activation. Orange ovals represent predicted upregulated metabolites. (B) The histamine degradation pathway. Upregulated proteins related to this pathway are represented by magenta framed diamonds. Note the fading of orange in aldehyde dehydrogenase; three out of six subunits were not considered differentially expressed ($P < 0.05$ and/or fold change between -1 and 1). Blue and magenta diamonds represent dots of the same colour in Figure 3A.
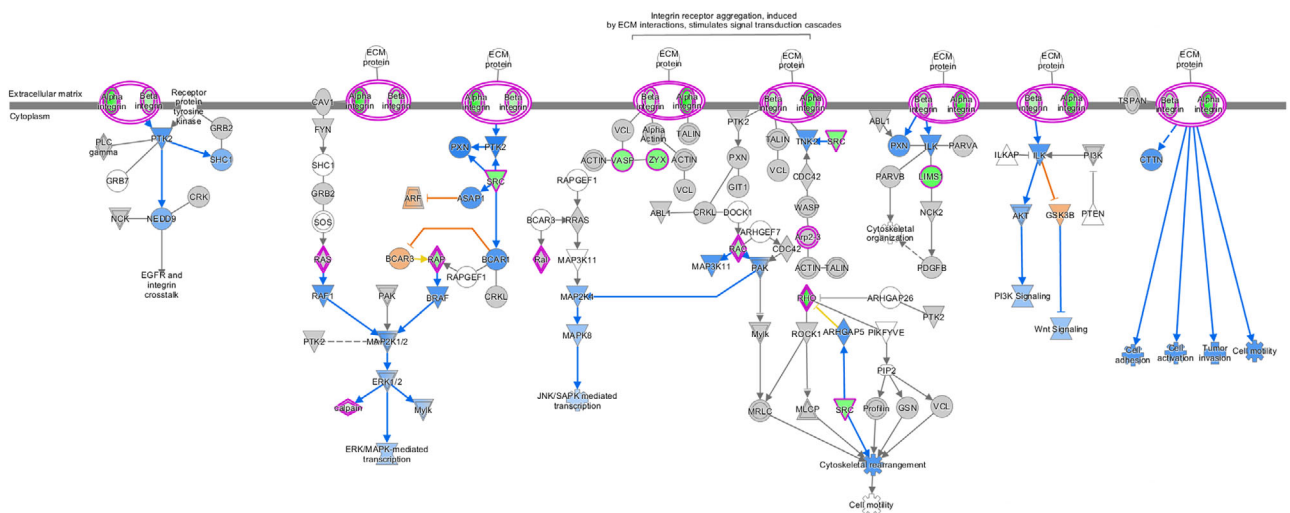
Figure 5. LCM thrombi analysis: Integrin signalling pathway. This pathway was significantly downregulated in COVID-19 thrombi. Magenta framed icons depict proteins and peptides identified in influenza and COVID-19 thrombi (see Figure 2B). Green icons portray identified down-regulated proteins in COVID-19 thrombi; blue and orange icons portray respectively down- and upregulated proteins or functions.

that being upregulation of EIF2 signalling and down-regulation of the 'deactivation of coronavirus pathogenesis' pathway. This pathway consisted of

nucleophosmin 1 (*NPM1*) and six ribosomal proteins (*RPS3/8/14/18/20/21*) (Figures 3C and 6B), which were all significantly upregulated in the *in situ*
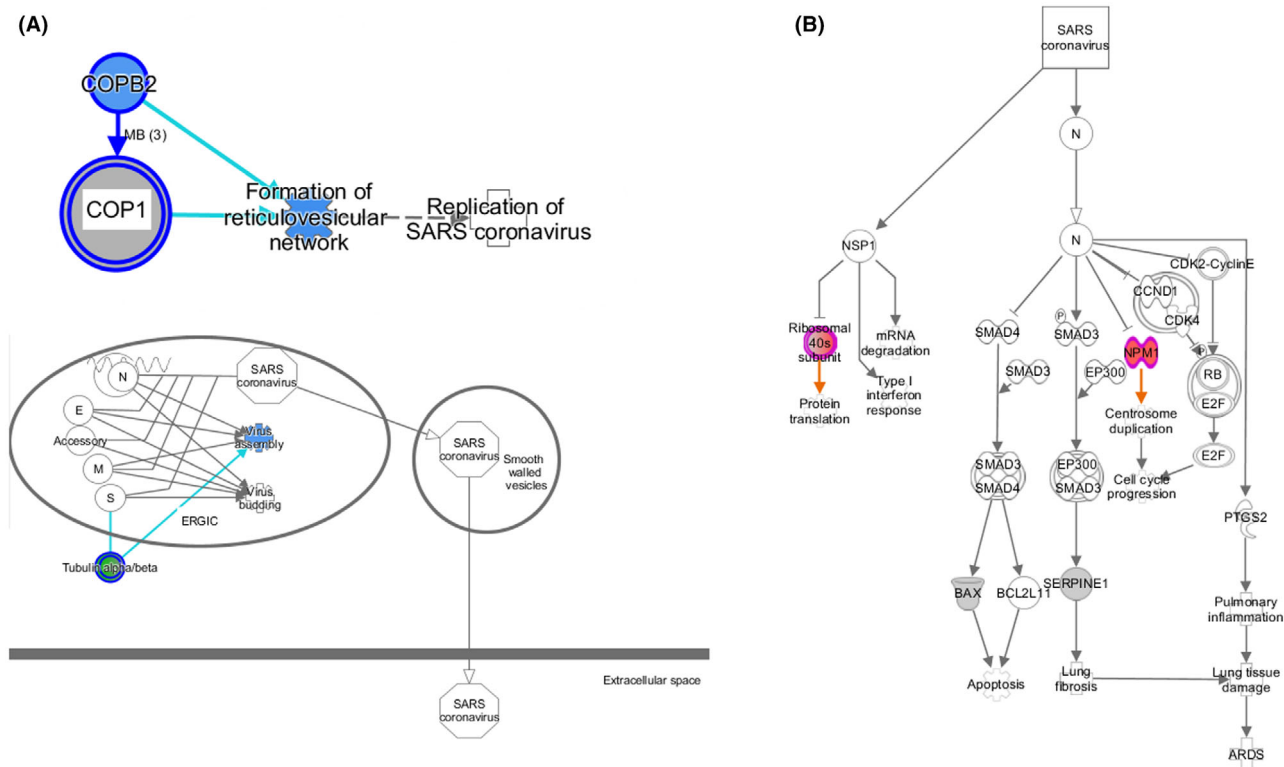
Figure 6. Coronavirus replication pathway (A) and coronavirus pathogenesis pathway (B) identified by IPA. (A) Downregulation of coronavirus replication pathway is based on virus assembly, although involved proteins are not pathognomonic for SARS coronavirus. Blue framed icons represent dots of the same colour in Figure 3B. (B) Downregulation of SARS CoV pathogenesis is based on increased levels of multiple Ribosomal 40s subunits and NPM1 by SARS coronavirus, ultimately leading to ARDS. Magenta framed circles represent identified upregulated proteins in COVID-19 thrombi.

thrombi group compared to the thromboemboli group (P-values varying between 0.007 and 0.029). However, these proteins showed no significant differential expression between influenza and COVID-19 thrombi, independent of thrombus type. *In situ* thrombi also showed a significant increase in functions related to viral infection.

LASER CAPTURE MICRODISSECTION ANALYSIS: ENDOTHELIUM

Protein profiling of isolated endothelium identified 2366 different proteins among all samples. On average, 1130 proteins and peptides were identified, ranging between 891 to 1484 per sample. LCM analysis of endothelium based on underlying disease showed 149 differentially expressed proteins between endothelium from COVID-19 and influenza cases. With LCM analysis of endothelium surrounding thrombi of different histomorphology, differentially 38 expressed proteins were identified between embolism and *in situ* cases.

Pathway analysis of endothelium stratified by disease identified differential expression of two pathways. The DHCR24 signalling pathway, involved in cholesterol synthesis, was upregulated in COVID-19 endothelium; the CSDE1 signalling pathway was downregulated. The activity of viral infection and replication was decreased in COVID-19 endothelium. There were no differentially expressed pathways regarding coagulation, thrombocytopenia, or haemostasis. Regarding analysis of protein expression between endothelium of vessels with either *in situ* thrombi or thromboemboli, no significant differentially expressed pathways were identified (Figure 3E). Similarly, no proteins related to specific diseases or functions showed significant differential expression.

Discussion

In this study we analysed proteins in postmortem lung tissue from severe COVID-19 and severe influenza patients, as well as isolated endothelium and

thrombi from pulmonary blood vessels through LC-MS. Although whole-tissue analysis predominantly showed upregulation of liver proteins, analysis of isolated COVID-19 thrombi showed downregulation of multiple platelet activity pathways that may indicate a relative increase in thromboembolism in COVID-19. Analysis of thrombi based on histomorphology showed upregulation of the coronavirus pathogenesis pathway in *in situ* thrombi, emphasizing the increase of *in situ* pulmonary thrombosis in COVID-19 as well.

DOWNREGULATED PLATELET PROTEINS IN ISOLATED COVID-19 THROMBI

Proteomics analysis of COVID-19 thrombi identified downregulation of various proteins related to coagulation compared to influenza thrombi (Intergrin, TGF-beta, thrombin, paxilin, ephrin, PAK, and CXCR4 signalling). The integrin signalling pathway was the most downregulated, which plays a vital role in platelet adhesion and aggregation at sites of endothelial damage.[10,11] A decrease of integrin and other platelet-related proteins in COVID-19 thrombi compared to influenza thrombi may indicate a thrombus origin. Integrin signalling has been described to have a key role in thrombosis in arteries[12,13]; downregulation of the integrin signalling pathway could thus mean a relative decrease of arterial *in situ* thrombosis. Additionally, the decrease of platelet transmembrane proteins integrin and ephrin in thrombi suggests an overall reduction of platelets in COVID-19 thrombi, as arterial thrombi contain more platelets compared to venous thrombi.[14,15] These findings imply that, in general, thrombi in COVID-19 are more often of venous origin compared to other diseases with pulmonary thrombi. A meta-analysis of thrombosis in COVID-19 supports our findings, reporting a high incidence of venous thromboembolic events in COVID-19 compared to similar lung diseases.[16] Lastly, ephrin signalling was upregulated in the whole-tissue analysis of COVID-19 lung tissue, suggesting that COVID-19 lung tissue taken as a whole has increased platelet activity. Thus, our data of these proteomics analyses strengthen the hypothesis that there is a relative increased risk of increased venous thromboembolism in COVID-19 compared to other diseases with pulmonary thrombi.

Multiple pathways related to inflammatory activity were also downregulated in thrombi of COVID-19 cases. These findings might contradict previous studies, as both these inflammatory pathways and previously mentioned pathways related to platelet activity were upregulated in COVID-19 serum samples.[17–27] We are not sure that measurement in serum can be directly compared to tissue. However, in general a reduction in platelet activity may occur in severe COVID-19. Recent studies found impaired integrin activity in platelet of COVID-19 patients versus healthy controls, with a more pronounced decline of integrin alpha IIb in severe COVID-19 patients.[28,29] Additionally, thrombocytopenia in COVID-19 was found to have a varying incidence of 23% to 36%, with increasing incidence in more severe cases, possibly as a result of a hypercoagulative state before endstage COVID-19.[30–32] A similar phenomenon regarding certain cytokine signalling pathways may also occur. Neutrophil exhaustion was seen in patients dying of COVID-19, which may explain the decrease of interleukin-8 signalling activity.[33,34] Thus, a state of leukocyte and platelet depletion after cytokine storms and a hypercoagulation phase cannot be excluded.

CORONAVIRUS PATHWAYS IN ISOLATED THROMBI

Analysis of thrombi based on histomorphology, *in situ* thrombus, or thromboembolus found significant downregulation of coronavirus pathogenesis pathway in the latter, which IPA was based on upregulation of the following seven proteins: *NPM1* and ribosomal proteins *RPS3/8/14/18/20/21*. These ribosomal proteins are all part of ribosome subunit 40s, which monitors tRNA and mRNA to protein translation. Nonstructural proteins of SARS-CoV-2 (*NSP1*) binds to ribosome subunit 40, which inhibits its function. Thus, upregulation of these ribosomal proteins may imply intact function. However, several counterarguments can be made against the predicted downregulation of coronavirus pathogenesis. First, ribosomal proteins 3, 8, 14, 18, 20, and 21 were also found to be potential biomarkers for SARS-CoV-2 infection.[35–38] Second, *NPM1* (nucleolar phosphoprotein B23) is involved in key steps of replication of RNA and DNA viruses.[39] Therefore, upregulation of *NPM1* and ribosomal proteins *RPS3/8/14/18/20/21* instead suggests coronavirus pathogenesis activity in *in situ* thrombi.

Analysis of proteins in thrombi sorted by disease also revealed downregulation of the coronavirus replication pathway in COVID-19 thrombi compared to influenza thrombi based on the decrease of four proteins: COPI coat complex subunits alpha and gamma 1 (*COPA* and *COPG1*), as well as tubulin proteins (*TUBB1*, *TUBB6*, and *TUBB2A*). SARS-CoV-2 hijacks coatomer protein for replication,[40] while microtubules allow intracellular transport for SARS-CoV-2 to happen.[41,42] However, influenza virus also utilizes microtubules for intracellular transport, as both

destabilization of microtubules and COPI-complex depletion in severe cases resulted in defects of internalization of influenza.[43–45] Thus, downregulation of these proteins in COVID-19 may be a result of more extensive viral load in the endothelium of pulmonary blood vessels.

ORGAN FAILURE IN COVID-19

The high expression of proteins and pathways related to the liver in COVID-19 tissue and isolated COVID-19 endothelium may be a result of multiple organ failure. Liver failure in hospitalized COVID-19 patients is seen more often compared to influenza patients.[46,47] Although liver failure was clinically present in both groups (two out of eight COVID-19 cases and 3/11 influenza cases), no significant differential expression of liver proteins was found between patients with or without liver failure. Second, aldehyde dehydrogenase is also highly expressed in fat[48]; obesity was found to be a risk factor for COVID-19 and associated with increased severity of COVID-19,[49,50] which was not uncommon in COVID-19 patients included for this study: three out of eight COVID-19 cases had a BMI >30 compared to 1 out of 11 influenza patients.

Still, some of the upregulated pathways give insight into the pathophysiology of COVID-19 despite the presence liver proteins. A histamine degradation pathway was among the top three upregulated pathways in COVID-19 tissue, with seven corresponding differentially expressed proteins including (Figure 4) histamine N-methyltransferase (*HNMT*). Histamine has been found to induce proinflammatory cytokines and provoking endothelial damage in COVID19.[51–53] Our results are in line with these findings and imply increased mast cell activity, which may contribute to pulmonary fibrosis and thrombosis in COVID-19.[54,55] Upregulation of arginase (*ARG1*) in COVID-19 patients may also contribute to organ failure and pulmonary fibrosis. Arginase was also found to be increased in blood samples of intubated COVID-19 patients,[56–58] which is able to induce (pulmonary) fibrosis by indirectly promoting fibroblast proliferation and collagen production.[59–61] Thus, the influx of arginase in lung tissue may also play a role in fibrosis of endstage COVID-19.

LIMITATIONS

There were some limitations to this study. First, criteria for differentiating *in situ* thrombi and thromboemboli were based on expert opinion and not validated clinically. Differentiation between these

phenotypes of thrombi based on these histomorphological thrombus were also hard to appreciate in microthrombi >100 μm. Additionally, since HE slides represent a three-dimensional structure by a two-dimensional image, classification of thrombi based on histology are prone to sampling error. Thus, the results of this study should be interpreted with caution. Future studies should evaluate the clinical significance of this classification. Second, there was some selection bias. A small fraction of lung tissue was sampled and analysed with pathway analysis tools that were not all validated with orthogonal techniques. In addition, only lung tissue samples of severe COVID-19 and severe influenza in their lethal stage were used for this study. Inherent to the design of this study, performed analyses could only display protein expression at one instance in time. No correlation could be made between alterations in patient health and biomarker levels during admission. Data from COVID cases in this study would most likely be infected with the alpha variant of SARS-CoV-2. Since it is unknown if similar results would apply for other variants or milder phenotypes, the results of this study should be interpreted with caution. The difference in age between influenza and COVID-19 patients may have also influenced some difference in the identified proteins. Third, while laser microdissection was able to accurately isolate thrombi, inclusion of smooth muscle tissue and occasional intravascular erythrocytes for endothelium analysis was unavoidable. Lastly, influenza type from one case could not be retrieved from available patient data.

Conclusion

Deep venous thrombosis and pulmonary thromboembolism play a vital role in COVID-19 pathophysiology and clinical outcome. While proteomics profiling of SARS-CoV-2 infected lung tissue and isolated endothelium predominantly shows upregulation of liver metabolism pathways in severe COVID-19, which may play a role in pulmonary fibrosis, analysis of isolated thrombi show a decrease of platelet activation proteins and pathways in COVID-19 thrombi compared to influenza thrombi. This may suggest a relative increase in classic venous thromboembolism in severe COVID-19 compared to other diseases with pulmonary thrombi. Based on histomorphology, *in situ* thrombi show upregulation of SARS-CoV-2 pathogenesis proteins compared to thromboemboli, which may indicate increased *in situ* pulmonary thrombosis in COVID-19. Therefore, this study supports the

increase of venous thromboembolism without under-cutting the involvement of *in situ* thrombosis in severe COVID-19 at a molecular level.

Author contributions

BL: study design, tissue acquisition and processing, data interpretation and figures, main writer. CG: performed liquid chromatography and mass spectrometry and analytic calculations. AL: tissue processing and data interpretation. TB: tissue processing. FK, MH, and MK: revision of the article. JT and TL: study design, data analysis and interpretation, supervision and main reviewers of the text. All authors have read and approved the current version of the article.

Funding information

Conflict of interest

MV Huisman reports unrestricted grant support from The Netherlands Organization for Health Research and Development (ZonMW), and unrestricted grant support and fees for presentations from Boehringer-Ingelheim, Pfizer-BMS, Bayer Health Care, Aspen, Daiichi-Sankyo, all outside the submitted work. MHJA Kruip reports unrestricted research grants from Bayer, Boehringer-Ingelheim, Daiichi-Sankyo, all outside the submitted work. The Dutch COVID Pathology Consortium is supported by The Netherlands Organization for Health Research and Development (ZonMw). The Dutch COVID & Thrombosis Coalition is supported by The Netherlands Organization for Health Research and Development (ZonMw) and the Dutch Thrombosis Association.

Ethics approval and consent to participate

Consent was by the next of kin to utilize postmortem organ tissue from autopsies for research purposes. Permission for utilization of COVID-19 tissue samples was granted by the Medical Ethics Review Committee (MEC-2020-0322).

Data availability statement

The data that support the findings of this study are available from the corresponding author upon reasonable request.

References

1. World Health Organization. The true death toll of COVID-19: estimating global excess mortality. 2023 https://www.who.int/data/stories/the-true-death-toll-of-covid-19-estimating-global-excess-mortality.
2. Paget J, Spreeuwenberg P, Charu V *et al.* Global mortality associated with seasonal influenza epidemics: new burden estimates and predictors from the GLaMOR project. *J. Glob. Health* 2019; **9**; 020421.
3. Piroth L, Cottenet J, Mariet AS *et al.* Comparison of the characteristics, morbidity, and mortality of COVID-19 and seasonal influenza: a nationwide, population-based retrospective cohort study. *Lancet Respir. Med.* 2021; **9**; 251–259.
4. Hanff TC, Mohareb AM, Giri J, Cohen JB, Chirinos JA. Thrombosis in COVID-19. *Am. J. Hematol.* 2020; **95**; 1578–1589.
5. Stals MAM, Grootenboers M, van Guldener C *et al.* Risk of thrombotic complications in influenza versus COVID-19 hospitalized patients. *Res. Pract. Thromb. Haemost.* 2021; **5**; 412–420.
6. Baranga L, Khanuja S, Scott JA *et al.* In situ pulmonary arterial thrombosis-literature review and clinical significance of a distinct entity. *AJR Am. J. Roentgenol.* 2023; **221**; 57–68.
7. Gorog DA, Storey RF, Gurbel PA *et al.* Current and novel biomarkers of thrombotic risk in COVID-19: a Consensus Statement from the International COVID-19 Thrombosis Biomarkers Colloquium. *Nat. Rev. Cardiol.* 2022; **19**; 475–495.
8. Taubenberger JK, Morens DM. The pathology of influenza virus infections. *Annu. Rev. Pathol.* 2008; **3**; 499–522.
9. Armstrong SM, Darwish I, Lee WL. Endothelial activation and dysfunction in the pathogenesis of influenza a virus infection. *Virulence* 2013; **4**; 537–542.
10. Lavergne M, Janus-Bell E, Schaff M, Gachet C, Mangin PH. Platelet integrins in tumor metastasis: do they represent a therapeutic target? *Cancers (Basel)* 2017; **9**; 133.
11. Calderwood DA. Integrin activation. *J. Cell Sci.* 2004; **117**(Pt 5); 657–666.
12. Huang J, Li X, Shi X *et al.* Platelet integrin $\alpha IIb\beta 3$: signal transduction, regulation, and its therapeutic targeting. *J. Hematol. Oncol.* 2019; **12**; 26.
13. Zou J, Swieringa F, de Laat B, de Groot PG, Roest M, Heemskerk JWM. Reversible platelet integrin $\alpha IIb\beta 3$ activation and thrombus instability. *Int. J. Mol. Sci.* 2022; **23**; 12512.
14. Koupenova M, Kehrel BE, Corkrey HA, Freedman JE. Thrombosis and platelets: an update. *Eur. Heart J.* 2017; **38**; 785–791.
15. Jerjes-Sanchez C. Venous and arterial thrombosis: a continuous spectrum of the same disease? *Eur. Heart J.* 2005; **26**; 3–4.
16. Kunutsor SK, Laukkanen JA. Incidence of venous and arterial thromboembolic complications in COVID-19: a systematic review and meta-analysis. *Thromb. Res.* 2020; **196**; 27–30.

17. Fard MB, Fard SB, Ramazi S, Atashi A, Eslamifar Z. Thrombosis in COVID-19 infection: role of platelet activation-mediated immunity. *Thromb. J.* 2021; **19**; 59.

18. Barrett TJ, Bilaloglu S, Cornwell M *et al*. Platelets contribute to disease severity in COVID-19. *J. Thromb. Haemost.* 2021; **19**; 3139–3153.

19. Jevtic SD, Nazy I. The COVID complex: a review of platelet activation and immune complexes in COVID-19. *Front. Immunol.* 2022; **13**; 807934.

20. Yatim N, Boussier J, Chocron R *et al*. Platelet activation in critically ill COVID-19 patients. *Ann. Intensive Care* 2021; **11**; 113.

21. Li L, Li J, Gao M *et al*. Interleukin-8 as a biomarker for disease prognosis of coronavirus Disease-2019 patients. *Front. Immunol.* 2020; **11**; 602395.

22. Shouib R, Eitzen G. Cdc42 regulates cytokine expression and trafficking in bronchial epithelial cells. *Front. Immunol.* 2022; **13**; 1069499.

23. Al-Kuraishy HM, Al-Gareeb AI, Alkazmi L, Habotta OA, Batiha GE. High-mobility group box 1 (HMGB1) in COVID-19: extrapolation of dangerous liaisons. *Inflammopharmacology* 2022; **30**; 811–820.

24. Wulandari S, Hartono, Wibawa T. The role of HMGB1 in COVID-19-induced cytokine storm and its potential therapeutic targets: a review. *Immunology* 2023; **169**; 117–131.

25. Chang Z, Wang Y, Zhou X, Long JE. STAT3 roles in viral infection: antiviral or proviral? *Future Virol.* 2018; **13**; 557–574.

26. Matsuyama T, Kubli SP, Yoshinaga SK, Pfeffer K, Mak TW. An aberrant STAT pathway is central to COVID-19. *Cell Death Differ.* 2020; **27**; 3209–3225.

27. Tian M, Liu W, Li X *et al*. HIF-1α promotes SARS-CoV-2 infection and aggravates inflammatory responses to COVID-19. *Signal Transduct. Target. Ther.* 2021; **6**; 308.

28. Goudswaard LJ, Williams CM, Khalil J *et al*. Alterations in platelet proteome signature and impaired platelet integrin α (IIb)β(3) activation in patients with COVID-19. *J. Thromb. Haemost.* 2023; **21**; 1307–1321.

29. Ercan H, Schrottmaier WC, Pirabe A *et al*. Platelet phenotype analysis of COVID-19 patients reveals progressive changes in the activation of integrin αIIbβ3, F13A1, the SARS-CoV-2 target EIF4A1 and Annexin A5. *Front. Cardiovasc. Med.* 2021; **8**; 779073.

30. Guan WJ, Ni ZY, Hu Y *et al*. Clinical characteristics of coronavirus disease 2019 in China. *N. Engl. J. Med.* 2020; **382**; 1708–1720.

31. Asrie F, Tekle E, Gelaw Y *et al*. Baseline thrombocytopenia and disease severity among COVID-19 patients, Tibebe Ghion specialized hospital COVID-19 treatment center, Northwest Ethiopia. *J. Blood Med.* 2022; **13**; 315–325.

32. Bhattacharjee S, Banerjee M. Immune thrombocytopenia secondary to COVID-19: a systematic review. *SN Compr. Clin. Med.* 2020; **2**; 2048–2058.

33. Loyer C, Lapostolle A, Urbina T *et al*. Impairment of neutrophil functions and homeostasis in COVID-19 patients: association with disease severity. *Crit. Care* 2022; **26**; 155.

34. Qazi BS, Tang K, Qazi A. Recent advances in underlying pathologies provide insight into interleukin-8 expression-mediated inflammation and angiogenesis. *Int. J. Inflam.* 2011; **2011**; 908468.

35. Vastrad B, Vastrad C, Tengli A. Bioinformatics analyses of significant genes, related pathways, and candidate diagnostic biomarkers and molecular targets in SARS-CoV-2/COVID-19. *Gene Rep.* 2020; **21**; 100956.

36. Hasankhani A, Bahrami A, Sheybani N *et al*. Differential Co-expression network analysis reveals key hub-high traffic genes as potential therapeutic targets for COVID-19 pandemic. *Front. Immunol.* 2021; **12**; 789317.

37. Wu C, Wu Z, Chen Y, Huang X, Tian B. Potential core genes associated with COVID-19 identified via weighted gene co-expression network analysis. *Swiss Med. Wkly.* 2022; **152**; 40033.

38. Li G, He X, Zhang L *et al*. Assessing ACE2 expression patterns in lung tissues in the pathogenesis of COVID-19. *J. Autoimmun.* 2020; **112**; 102463.

39. Lobaina Y, Perera Y. Implication of B23/NPM1 in viral infections, potential uses of B23/NPM1 inhibitors as antiviral therapy. *Infect. Disord. Drug Targets* 2019; **19**; 2–16.

40. Dey D, Singh S, Khan S *et al*. An extended motif in the SARS-CoV-2 spike modulates binding and release of host coatomer in retrograde trafficking. *Commun. Biol.* 2022; **5**; 115.

41. Aminpour M, Hameroff S, Tuszynski JA. How COVID-19 hijacks the cytoskeleton: therapeutic implications. *Life (Basel)* 2022; **12**; 814.

42. Wen Z, Zhang Y, Lin Z, Shi K, Jiu Y. Cytoskeleton-a crucial key in host cell for coronavirus infection. *J. Mol. Cell Biol.* 2020; **12**; 968–979.

43. Simpson C, Yamauchi Y. Microtubules in influenza virus entry and egress. *Viruses* 2020; **12**; 117.

44. De Conto F, Chezzi C, Fazzi A *et al*. Proteasomes raise the microtubule dynamics in influenza A (H1N1) virus-infected LLC-MK2 cells. *Cell. Mol. Biol. Lett.* 2015; **20**; 840–866.

45. Sun E, He J, Zhuang X. Dissecting the role of COPI complexes in influenza virus infection. *J. Virol.* 2013; **87**; 2673–2685.

46. Shafran N, Issachar A, Shochat T, Shafran IH, Bursztyn M, Shlomai A. Abnormal liver tests in patients with SARS-CoV-2 or influenza - prognostic similarities and temporal disparities. *JHEP Rep.* 2021; **3**; 100258.

47. Yu D, Du Q, Yan S *et al*. Liver injury in COVID-19: clinical features and treatment management. *Virol. J.* 2021; **18**; 121.

48. Wang W, Wang C, Xu H, Gao Y. Aldehyde dehydrogenase, liver disease and cancer. *Int. J. Biol. Sci.* 2020; **16**; 921–934.

49. Alberca RW, Oliveira LM, Branco A, Pereira NZ, Sato MN. Obesity as a risk factor for COVID-19: an overview. *Crit. Rev. Food Sci. Nutr.* 2021; **61**; 2262–2276.

50. Chu Y, Yang J, Shi J, Zhang P, Wang X. Obesity is associated with increased severity of disease in COVID-19 pneumonia: a systematic review and meta-analysis. *Eur. J. Med. Res.* 2020; **25**; 64.

51. Raghavan S, Leo MD. Histamine potentiates SARS-CoV-2 spike protein entry into endothelial cells. *Front. Pharmacol.* 2022; **13**; 872736.

52. Kakavas S, Karayiannis D, Mastora Z. The complex interplay between immunonutrition, mast cells, and histamine signaling in COVID-19. *Nutrients* 2021; **13**; 3458.

53. Ennis M, Tiligada K. Histamine receptors and COVID-19. *Inflamm. Res.* 2021; **70**; 67–75.

54. Murdaca G, Di Gioacchino M, Greco M *et al*. Basophils and mast cells in COVID-19 pathogenesis. *Cell* 2021; **10**; 2754.

55. Budnevsky AV, Avdeev SN, Kosanovic D *et al*. Role of mast cells in the pathogenesis of severe lung damage in COVID-19 patients. *Respir. Res.* 2022; **23**; 371.

56. Derakhshani A, Hemmat N, Asadzadeh Z *et al*. Arginase 1 (Arg1) as an up-regulated gene in COVID-19 patients: a

promising marker in COVID-19 immunopathy. *J. Clin. Med.* 2021; **10**; 1051.

57. Thomas T, Stefanoni D, Reisz JA *et al.* COVID-19 infection alters kynurenine and fatty acid metabolism, correlating with IL-6 levels and renal status. *JCI Insight* 2020; **5**; e140327.

58. Sekine S, Ogawa R, McManus MT, Kanai Y, Hebrok M. Dicer is required for proper liver zonation. *J. Pathol.* 2009; **219**; 365–372.

59. Munder M. Arginase: an emerging key player in the mammalian immune system. *Br. J. Pharmacol.* 2009; **158**; 638–651.

60. Caldwell RW, Rodriguez PC, Toque HA, Narayanan SP, Caldwell RB. Arginase: a multifaceted enzyme important in health and disease. *Physiol. Rev.* 2018; **98**; 641–665.

61. Mora AL, Torres-González E, Rojas M *et al.* Activation of alveolar macrophages via the alternative pathway in herpesvirus-induced lung fibrosis. *Am. J. Respir. Cell Mol. Biol.* 2006; **35**; 466–473.

Supporting Information

Additional Supporting Information may be found in the online version of this article:

Table S1. List of identified proteins per analysis with corresponding accession number and *P*-value after ANOVA test between the two groups; per analysis.

Table S2. List of identified pathways by IPA per analysis with corresponding −log *P*-value, ratio, *z*-score and identified proteins; per analysis.